6-27-2003

Quantum Dynamics of a Hydrogen Molecule Confined in a Cylindrical Potential

Taner Yildirim
University of Pennsylvania, taner@seas.upenn.edu

A. Brooks Harris
University of Pennsylvania, harris@sas.upenn.edu

Recommended Citation

Yildirim, T., & Harris, A. (2003). Quantum Dynamics of a Hydrogen Molecule Confined in a Cylindrical Potential. *Physical Review B*, 37 245413-1-245413-15. http://dx.doi.org/10.1103/PhysRevB.67.245413

At the time of publication, author Taner Yildirim was affiliated with the National Institute of Standards and Technology, Gaithersburg, Maryland. Currently, he is a faculty member in the Materials Science and Engineering Department at the University of Pennsylvania.

Quantum Dynamics of a Hydrogen Molecule Confined in a Cylindrical Potential

Abstract
We study the coupled rotation-vibration levels of a hydrogen molecule in a confining potential with cylindrical symmetry. We include the coupling between rotations and translations and show how this interaction is essential to obtain the correct degeneracies of the energy level scheme. We applied our formalism to study the dynamics of H_2 molecules inside a "smooth" carbon nanotube as a function of tube radius. The results are obtained both by numerical solution of the $(2J+1)$-component radial Schrödinger equation and by developing an effective Hamiltonian to describe the splitting of a manifold of states of fixed angular momentum J and number of phonons N. For nanotube radius smaller than ≈3.5Å, the confining potential has a parabolic shape and the results can be understood in terms of a simple toy model. For larger radius, the potential has the "Mexican hat" shape and therefore the H_2 molecule is off centered, yielding radial and tangential translational dynamics in addition to rotational dynamics of H_2 molecule which we also describe by a simple model. Finally, we make several predictions for the the neutron scattering observation of various transitions between these levels.

Disciplines
Physics | Quantum Physics

Comments
At the time of publication, author Taner Yildirim was affiliated with the National Institute of Standards and Technology, Gaithersburg, Maryland. Currently, he is a faculty member in the Materials Science and Engineering Department at the University of Pennsylvania.

Quantum dynamics of a hydrogen molecule confined in a cylindrical potential

Taner Yildirim
National Institute of Standards and Technology, Gaithersburg, Maryland 20899, USA

A. B. Harris
Department of Physics and Astronomy, University of Pennsylvania, Philadelphia, Pennsylvania 19104, USA

(Received 12 December 2002; published 27 June 2003)

We study the coupled rotation-vibration levels of a hydrogen molecule in a confining potential with cylindrical symmetry. We include the coupling between rotations and translations and show how this interaction is essential to obtain the correct degeneracies of the energy level scheme. We applied our formalism to study the dynamics of H_2 molecules inside a ''smooth'' carbon nanotube as a function of tube radius. The results are obtained both by numerical solution of the $(2J+1)$-component radial Schrödinger equation and by developing an effective Hamiltonian to describe the splitting of a manifold of states of fixed angular momentum J and number of phonons N. For nanotube radius smaller than ≈ 3.5 Å, the confining potential has a parabolic shape and the results can be understood in terms of a simple toy model. For larger radius, the potential has the ''Mexican hat'' shape and therefore the H_2 molecule is off centered, yielding radial and tangential translational dynamics in addition to rotational dynamics of H_2 molecule which we also describe by a simple model. Finally, we make several predictions for the the neutron scattering observation of various transitions between these levels.

DOI: 10.1103/PhysRevB.67.245413 PACS number(s): 78.70.Nx, 34.50.Ez, 82.80.Gk, 71.20.Tx

I. INTRODUCTION

The study of quantum dynamics of hydrogen molecules in confined geometries has recently developed into an active field both experimentally and theoretically[1–12] due to potential use as catalysts, molecular sieves, and storage media. In the case of fullerenes and nanotubes, such trapping may yield new exotic quantum systems due to zero and one dimensionality of the absorption sites, respectively. Thus, understanding the structural and dynamical aspects of trapping in confining geometries is of both fundamental and practical importance.

The theory of molecular rotation in solids has a long history dating back to the early work of Pauling,[13] Devonshire,[14] and Cundy.[15] They introduced the concept of the crystal field potential $V(\Omega)$, where Ω specifies the orientation of the molecule, to solve for the energy levels of the hindered rigid-rotor. This traditional approach assumes that the center of mass (c.m.) of the trapped molecules are fixed and therefore does not take into account the rotation-vibration (RV) coupling. However, recent studies[5,11] have indicated that vibrational levels of H_2 trapped in the octahedral sites of C_{60}, for example, are significantly perturbed by RV coupling and in a previous paper[5] (I) we have shown that this coupling has to be included in a symmetry analysis of the energy level degeneracies. Interestingly, to date there is a little done to treat c.m. dynamics and RV coupling. Most of the studies are based on the approximation where an effective orientational crystal field potential is obtained after the potential is averaged over the zero-point translational motions of the H_2 molecule.[11,12]

Recently (in I) we have presented a detailed theory of coupled RV dynamics of H_2 molecule trapped in a zero-dimensional cavity with various symmetries. Here we present a similar study to analyze the combined rotational and translation states of hydrogen molecules confined in a one-dimensional potential. This problem is closely related to the experimental situation where hydrogen molecules are absorbed into carbon nanotube ropes. Figure 1 shows schematically various types of absorption sites for H_2 molecule. Several neutron and Raman scattering experiments have been carried out to characterize the binding energies and rotational barriers for H_2 at these sites with conflicting results.[1–4,9–11] One of the motivations of the present work is to provide a detailed description of the RV dynamics of H_2 molecules at these different absorption sites and discuss the consequences

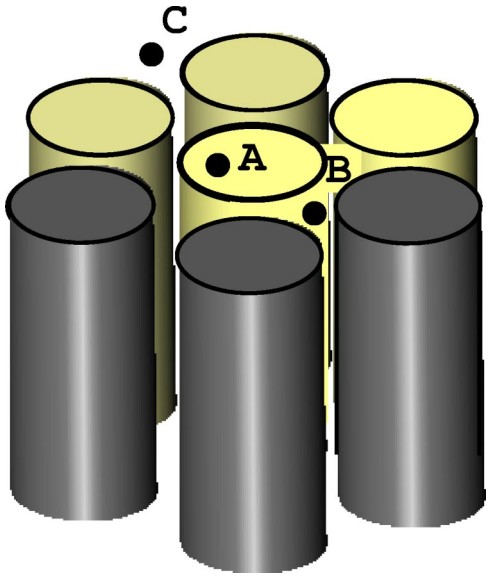

FIG. 1. A schematic representation of a single wall carbon nanotube rope indicating three different absorption sites, namely, (A) endohedral, (B) interstitial, and (C) external adsorption sites, respectively.

for inelastic neutron scattering experiments. In the present paper, we focus our attention on the general formalism and discuss only the case where a single H_2 is confined inside a single nanotube. Extension of this work to the interstitial and external sites and to cases where H_2 molecules interact with one another will be presented elsewhere.

Briefly this paper is organized as follows. In the next section, we discuss the potential model for hydrogen and nanotube interactions and validate several approximations, such as assuming a smooth tube, used in our formalism. In Sec. III we present our formalism to treat the coupled rotational and translational motion of H_2 molecule confined in a smooth nanotube. We show that the problem can be mapped into a $(2J+1)$-component radial Schrödinger equation which can be solved numerically. In Sec. IV we discuss the dynamics of a hydrogen molecule when the confining potential has parabolic shape (which occurs for a small-radius nanotube). We interpret the exact numerical results in terms of a simple analytical toy model. In Sec. V we discuss the case where the confining potential has a Mexican-hat shape. For this case [which occurs for large radius nanotubes such as (10,10)] the equilibrium position of the c.m. of the H_2 molecule is off-center and it performs radial and tangential translational oscillation in combination with its rotational dynamics. In this section, we also present several perturbation results which help to interpret the exact numerical results. In Sec. VI we discuss the experimental observation of various transitions via inelastic neutron scattering measurements. Our conclusions are summarized in Sec. VII.

II. POTENTIAL MODEL

We model the intermolecular potential for H_2 trapped in a carbon nanotube as a sum of atom-atom potentials

$$V(\mathbf{r},\Omega)=\sum_{i,H}\sum_{j,C}\left[B\exp(-Cr_{ij})-A/r_{ij}^6\right]. \qquad (1)$$

The dependence of the potential on the position $(\mathbf{r})$ and orientation (Ω) of H_2 molecule is through the interatomic distances r_{ij}. All the results reported in this paper are obtained from the same WS77 potential[16] $-A/r^6+B\exp(-Cr)$ (where $A=5.94$ eV Å,[6] $B=678.2$ eV, and $C=3.67$ Å^{-1}), that we used in I.[5] Compared to other commonly used potentials, the WS77 potential gave the best fit to the energy spectrum of H_2 in solid C_{60}.

For simplicity we will restrict this formulation to the idealized case when the hydrogen molecule is confined by a so-called ''smooth'' nanotube. By this we mean that the potential produced by the nanotube has cylindrical symmetry and is invariant with respect to translations along its axis of symmetry. In some of our numerical work we will study ''real'' nanotubes which do not possess the high symmetry of ''smooth'' nanotubes.

It is instructive to look at various potentials for an orientationally averaged hydrogen molecule (i.e., parahydrogen with $J=0$) when H_2 is inside and outside a single nanotube. Figure 2 indicates two different types of confining potential depending on the nanotube radius. Figure 2 shows that for small nanotubes such as (9,0), the potential minimum occurs at the center of the tube and therefore the potential has a parabolic shape. However, for larger nanotubes such as the (10,10) nanotube, the minimum is off centered and therefore the potential has a Mexican-hat shape. Because of this off centering the dynamics of the H_2 molecule is a quite interesting and rich one as we discuss in detail below. The right panels in Fig. 2 shows the potential when the H_2 molecule is outside the nanotubes. The outside binding energy does not depend on the tube radius strongly and is about 30 meV. The horizontal lines indicates the radial phonon energy levels, indicating that at least a few bound states can occur even for a hydrogen molecule outside a single nanotube. The solid and dashed lines in Fig. 2 show the results with and without the smooth tube approximation, respectively. Since these two curves are very close to one another, the smooth tube approximation will not cause significant error in our theory.

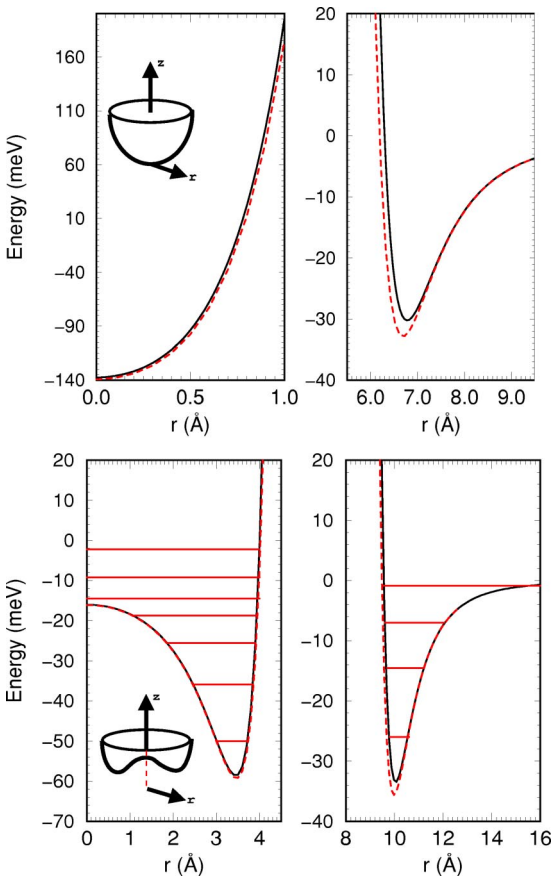

FIG. 2. Potential energy as a function of distance from tube center for a para hydrogen (i.e., $J=0$) interacting with a (9,0) (top) and (10,10) (bottom) nanotube. The solid and dashed lines are for smooth and actual carbon nanotubes, respectively. For the actual carbon nanotubes, the value of z axis is taken arbitrarily. The horizontal lines in the bottom panel indicate the radial phonon bound states in smooth nanotubes. The insets to the left panels are schematic plots of the parabolic (top) and Mexican hat potentials, respectively.

In order to develop some intuition about the orientational potential for a hydrogen molecule in a nanotube, in Fig. 3(a) we show the radial potential for three different orientations

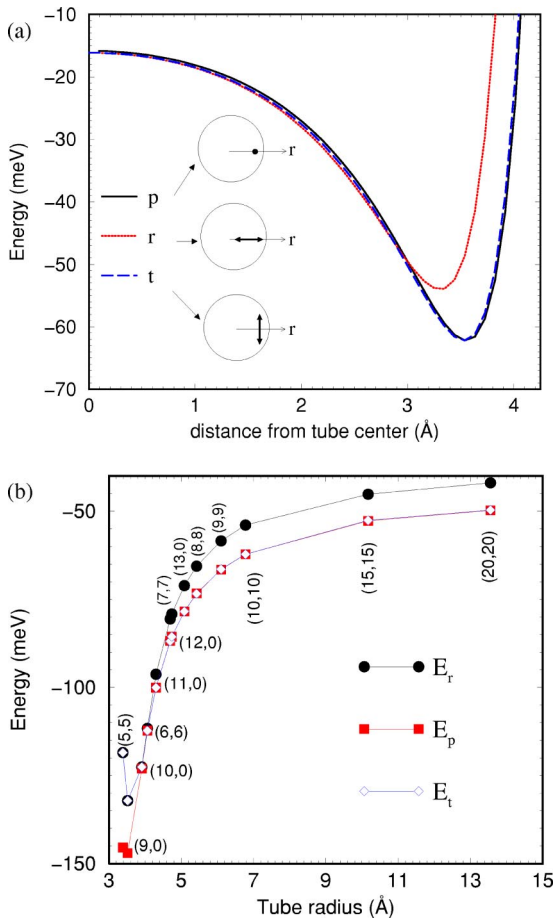

FIG. 3. (a) Potential energy as a hydrogen molecule is translated from the center of a (10,10) nanotube when H_2 is oriented to be parallel to the tube axis (p), radially (r), and tangentially (t), respectively. Inset shows these configurations. The equilibrium distance and minimum potential depends strongly on the orientation of the H_2 molecule, indicating strong rational-translational coupling. (b) The minimum potential energies E_r, E_p, and E_t, for radial, parallel, and tangential orientation of H_2 molecule for various nanotubes.

of H_2 molecule inside a (10,10) nanotube. We note that the radius of the (10,10) tube is large enough that the parallel to the axis (p) and tangential (t) orientations [as depicted in the inset to Fig. 3(a)] give almost the same energy. However, the radial (r) orientation of a H_2 molecule has a minimum energy which is about 8 meV higher in energy than that of the other two orientations. We also point out that the position of the c.m. of the H_2 molecule for the minimum potential energy changes about 0.2 Å depending on the orientation of the H_2 molecule. This is a clear indication that the orientational and vibrational motion of hydrogen molecule are significantly coupled.

Figure 3(b) shows the minimum potential energies E_r, E_p, and E_t for respective radial, parallel, and tangential orientations of an H_2 molecule inside various nanotubes. It is clear that for nanotube radius around 3 Å, the orientational dependence of the potential is of the order of 30 meV and therefore is comparable to the energy separation of 80 meV or more between energy levels corresponding to different rotational quantum number J's. Accordingly, for tubes whose radius is less than that of a (9,0) tube, J may not be considered to be a good quantum number. For large nanotubes, such as (10,10), the orientational potential is of the order of 8 meV and does not change much with larger radius tubes (i.e., close to the graphite limit). In the present paper, we present our formalism using (9,0) and (10,10) nanotubes which represent the two potential regimes; namely the parabolic and Mexican-hat potentials, but for both tubes J is considered to be a good quantum number.

III. FORMULATION

The hydrogen molecule is unique in that its moment of inertia is small enough that the rotational kinetic energy often dominates the orientational potential in which the molecule is placed. Under these circumstances the rotational quantum number J is nearly a good quantum number and the effect of the orientational potential is to reduce the degeneracy of the $2J+1$ substates of a given J. (The generalization of the formulation we present below to the case when J is not a good quantum number will be presented elsewhere).[17] In the present case any eigenfunction describing the orientational and translation state of the molecule can be written in the form

$$\Psi(\mathbf{r},\Omega)=\psi(r,\phi_r;\Omega)e^{ikz}=\sum_{M=-J}^{J}\Phi_M^{J,k}(r,\phi_r)Y_J^M(\Omega)e^{ikz}, \tag{2}$$

where r, z, and ϕ_r are the cylindrical coordinates of the center-of-mass of the hydrogen molecule, Ω denotes its molecular orientation specified by angles θ and ϕ, and $Y_J^M(\Omega)$ is a spherical harmonic. We will refer to $\psi(r,\phi_r;\Omega)$ as the cylindrical RV wave function. For economy of notation we henceforth omit the superscripts J and k. Because Φ_M is allowed to depend arbitrarily on r and ϕ_r, this wave function takes into account the most general interaction between rotations and translations subject to the constraint that J is a good quantum number. In this notation, the Hamiltonian for a single hydrogen molecule (of mass m) with J and k fixed is written as

$$\mathcal{H}=-\frac{\hbar^2}{2m}\nabla^2+BJ(J+1)+V(\mathbf{r},\Omega), \tag{3}$$

where m is the mass of an H_2 molecule and $V(\mathbf{r},\Omega)$ is the orientational potential which, as indicated, also depends on position. For a smooth nanotube we may write the orientational potential energy as

$$V(\mathbf{r},\Omega)=V_0(r)+\sum_{L,M}V_L^M(r,\phi_r)Y_L^M(\theta,\phi), \tag{4}$$

where the sum is over $L>0$. Here θ is the angle between the H_2 molecular axis and the axis of the tube. Although the transverse direction for $\phi=0$ is arbitrary, it does have to coincide with that for $\phi_r=0$. Because the hydrogen molecule is centrosymmetric, only terms with L even appear in the potential. Also, because a smooth nanotube has a mirror plane perpendicular to the axis of symmetry, only terms with even M appear. Furthermore, because a global rotation of the

molecule (i.e., incrementing both ϕ and ϕ_r by the same amount) is a symmetry of the system, we may write

$$V(\mathbf{r},\Omega)=V_0(r)+\sum_{L,M} v_L^M(r)Y_L^M(\theta,0)e^{iM(\phi-\phi_r)}, \quad (5)$$

where v_L^M is a function only of r and $v_L^{-M}=v_L^{M}*$. In addition, $v_L^M(r=0)$ vanishes for $M\neq 0$. There is also a mirror plane containing the long axis of the tube which implies that the potential should be an even function of $(\phi-\phi_r)$. This implies that $v_L^M(r)$ is a real-valued function. This function may be evaluated by integrating the potential at a fixed center-of-mass position over all orientations

$$v_L^M(r)=e^{iM\phi_r}\int d\Omega\, Y_L^M(\theta,\phi)^*V(\mathbf{r},\Omega). \quad (6)$$

Contrary to appearance, $v_L^M(r)$ does not depend on ϕ_r because $V(\mathbf{r},\Omega)$ is a function of $(\phi-\phi_r)$.

The Schrödinger equation for $\psi(r,\phi_r;\Omega)$ is

$$\left[-\frac{\hbar^2}{2m}\left(\frac{\partial^2}{\partial r^2}+\frac{1}{r}\frac{\partial}{\partial r}+\frac{1}{r^2}\frac{\partial^2}{\partial\phi_r^2}\right)+V_0(r)+\sum_{LM} v_L^M(r)e^{-iM\phi_r}Y_L^M(\Omega)\right]\psi^{(\alpha)}(r,\phi_r;\Omega)=\hat{E}^{(\alpha)}\psi^{(\alpha)}(r,\phi_r;\Omega), \quad (7)$$

where $\hat{E}^{(\alpha)}=E^{(\alpha)}-BJ(J+1)-\hbar^2k^2/(2m)$. For given values of J and k, this equation generates a spectrum of eigenvectors $\psi^{(\alpha)}(r,\phi_r;\Omega)$ with associated eigenvalues $\hat{E}^{(\alpha)}$, for $\alpha=0,1,\ldots$. Substituting Eq. (2) into the Schrödinger equation we rewrite it in the form

$$\left\{-\frac{\hbar^2}{2m}\left(\frac{\partial^2}{\partial r^2}+\frac{1}{r}\frac{\partial}{\partial r}+\frac{1}{r^2}\frac{\partial^2}{\partial\phi_r^2}\right)+V_0(r)\right\}\Phi_M^{(\alpha)}(r,\phi_r)+\sum_{L,M'}\left(\int d\Omega\, Y_J^M(\Omega)^*Y_L^{M'}(\Omega)Y_J^{M-M'}(\Omega)d\Omega\right)\times v_L^{M'}(r)\Phi_{M-M'}^{(\alpha)}(r,\phi_r)e^{-iM'\phi_r}=\hat{E}^{(\alpha)}\Phi_M^{(\alpha)}(r,\phi_r),\quad M=-J,-J+1\cdots J-1,J. \quad (8)$$

We see that we may write a solution to this set of equations in the form

$$\Phi_M^{(\alpha)}(r,\phi_r)=f_{M,P}^{(\alpha)}(r)e^{-i(P+M)\phi_r}, \quad (9)$$

where P is a quantum number whose significance we will discuss shortly. Thus we have

$$\left\{-\frac{\hbar^2}{2m}\left(\frac{\partial^2}{\partial r^2}+\frac{1}{r}\frac{\partial}{\partial r}-\frac{1}{r^2}(P+M)^2\right)+V_0(r)\right\}f_{M,P}^{(\alpha)}(r)+\sum_{L,M'} v_L^{M'}(r)f_{M-M',P}^{(\alpha)}(r)\times\left(\int d\Omega\, Y_J^M(\Omega)^*Y_L^{M'}(\Omega)Y_J^{M-M'}(\Omega)d\Omega\right)=Ef_{M,P}^{(\alpha)}(r). \quad (10)$$

For each P index we have a Schrödinger equation for the $(2J+1)$-component wave function which is of the form $[f_{-J,P}^{(\alpha)}(r),f_{-J+1,P}^{(\alpha)}(r),\ldots f_{J,P}^{(\alpha)}(r)]$. Then the cylindrical RV wave function is

$$\psi_P^{(\alpha)}(r,\phi_r,\Omega)=e^{-iP\phi_r}\sum_M f_{M,P}^{(\alpha)}(r)Y_J^M(\Omega)e^{-iM\phi_r}=e^{-iP\phi_r}\sum_M f_{M,P}^{(\alpha)}(r)Y_J^M(\theta)e^{iM(\phi-\phi_r)}. \quad (11)$$

It is important to keep in mind that $v_L^M(r)$ vanishes for odd M. As a consequence, in the $(2J+1)$-component wave function there is no mixing between even and odd values of M. For $J=1$ wave functions one will have "even" wave functions in which the sum over M in Eq. (11) reduces to the single term for $M=0$ and "odd" wave functions in which the sum over M in Eq. (11) includes only $M=\pm 1$.

The quantum number P indicates that this wave function transforms as $e^{-iP\phi}$ when the position and orientation of the molecule are simultaneously rotated about the axis of symmetry. Under this global rotation the quantity

$$f_{M,P}^{(\alpha)}(r)e^{-iM\phi_r}Y_J^M(\Omega) \quad (12)$$

is invariant, so the total wave function transforms as stated. When $v_L^M(r)$ is independent of r, then, since $v_L^M(r=0)$ must vanish, we have that $v_L^M(r)=0$ for $M\neq 0$ and, in Eq (10) there is no coupling between $f_M^{(\alpha)}$'s for different values of M. Thus, in this case there is no dynamical interaction between the orientational coordinate and the center-of-mass coordinate and the wave function can be chosen so that $f_{M,P}$ is only nonzero for a single value of M. Then one has the usual separation of variables so that the orientational wave function is proportional to $e^{iM\phi}$ and the translation wave function is proportional to $e^{-i(M+P)\phi_r}$. Here we have accomplished a similar separation of coordinates when $v_L^M(r)$ is allowed to depend on r. Now the result is not a scalar radial equation, but rather a radial equation for a $(2J+1)$-component wave function. That is the result embodied in Eq. (10), where we have one such $(2J+1)$-component radial Schrödinger equation for each value of P.

IV. QUASIHARMONIC POTENTIAL

In this section we discuss the case exemplified by a H_2 molecule inside a (9,0) nanotube, for which the minimum of the potential $V_0(r)$ occurs for $r=0$, in which case we will

introduce a toy model with the isotropic harmonic potential $V_0(r)=\frac{1}{2}kr^2$.

A. No interactions between rotations and translations

1. Harmonic potential

Here we discuss the eigenvalues and eigenfunctions of the two-dimensional isotropic harmonic oscillator, to emphasize the relation between the above formulation in terms of cylindrical coordinates and that in terms of Cartesian coordinates. For an isotropic and harmonic potential we expect the eigenvalues to be

$$E_n=(n+1)\hbar\omega=(n+1)\sqrt{k/m}. \tag{13}$$

Note that the nth level (with energy $n\hbar\omega$) is n-fold degenerate, because in Cartesian notation, if, say $n=4$, we have wave functions (3,0), (2,1), (1,2), and (0,3), where (n,m) is a wave function with n excitations in the x coordinate and m excitations in the y coordinate. This degeneracy reflects the U_2 symmetry corresponding to the invariance of the Hamiltonian with respect to a transformation of the form

$$\begin{pmatrix}(a_x^\dagger)'\\(a_y^\dagger)'\end{pmatrix}=[\mathbf{U}]\begin{pmatrix}(a_x^\dagger)\\(a_y^\dagger)\end{pmatrix}, \tag{14}$$

where $a_x^\dagger$ and $a_y^\dagger$ create phonons in the x and y coordinates, respectively, and $\mathbf{U}$ is a two-dimensional unitary matrix. This transformation is essentially the same as a four-dimensional rotational symmetry in the space of the momenta p_x, p_y, and coordinates x and y. Since the kinetic energy is quadratic in the momenta, spherical symmetry in this space only holds if the potential is harmonic.

In cylindrical coordinates the eigenfunctions can be written as

$$\psi_\mu^\alpha(r)e^{i\mu\phi}, \tag{15}$$

where $\psi_\mu^\alpha(r)$ satisfies the radial equation

$$-\frac{\hbar^2}{2m}\left[\frac{d^2\psi_\mu^\alpha(r)}{dr^2}+\frac{1}{r}\frac{d\psi_\mu^\alpha(r)}{dr}-\frac{\mu^2}{r^2}\right]+\frac{1}{2}kr^2\psi_\mu^\alpha(r)=E_\mu^\alpha\psi_\mu^\alpha(r). \tag{16}$$

Here the family of solutions for a given value of μ are labeled $\alpha=0,1,2,\ldots$, in order of increasing energy and for the isotropic and harmonic potential we have

$$E_\mu^\alpha=(\mu+1+2\alpha)\hbar\omega. \tag{17}$$

So from the radial equation for $\mu=0$ we have eigenvalues $\hbar\omega$, $3\hbar\omega$, $5\hbar\omega$, etc. The fact that we have a seemingly accidental degeneracy between different representations (i.e., between different values of μ) is the result of the U_2 symmetry of the Hamiltonian mentioned above. A consequence of this symmetry is that for a harmonic potential the total energy depends only on the total number of phonon excitations. This symmetry is distinct from the circular symmetry in x-y space.

2. Anharmonic potential

The $U2$ symmetry is broken by anharmonic terms which then take us into the generic case of a particle in a circularly symmetric potential which is not harmonic. Accordingly, we now consider the effect of adding an anharmonic perturbation of the form γr^4 to the harmonic potential. For illustrative purposes, we treat this anharmonic perturbation within first-order perturbation theory. Our results are characteristic of the generic case, for which different values of m give rise to distinct eigenvalues. In this case, the n-fold degenerate manifold which has energy $n\hbar\omega$ for the harmonic potential is split into doublets (corresponding to the degeneracy between $+m$ and $-m$) and, if n is odd, a singlet from $m=0$. Our explicit results are given in Table I. These results are generic in the sense that addition of further anharmonic terms will not further change the degeneracies.

B. Toy model of translation-rotation coupling

In this section we explore the consequences of allowing coupling between rotations and translations. Since we now restrict attention to the manifold of $(J=1)$, we need keep only terms with $L=2$ in Eq. (5). Thus, as a toy model, we set

$$V(\mathbf{r},\Omega)=\frac{1}{2}kr^2-\frac{5}{2}\alpha(3\cos^2\theta-1)-\frac{5}{2}\beta r^2\sin^2\theta\cos(2\phi-2\phi_r), \tag{18}$$

where α, β, and k are constants and the factor $-\frac{5}{2}$ is included so that the matrix elements are numerically simple. Also we take the dependence on r to be quadratic to facilitate calculation of the matrix elements. In the language of Eq. (5) this model has $v_2^0(r)=-\alpha\sqrt{20\pi}$ and $v_2^{\pm 2}(r)=-\beta r^2\sqrt{10\pi/3}$. We are going to consider the effect of this Hamiltonian within the manifold of $(J=1)$ states. Using this toy model we can illustrate how the rotation-translation affects the symmetry of the energy levels. Within the $(J=1)$ manifold we may use operator equivalents to write

$$\begin{aligned}V(\mathbf{r},\Omega)&=\frac{1}{2}kr^2+\alpha(3J_z^2-2)+\beta[(J_x^2-J_y^2)(x^2-y^2)\\&\quad+2(J_xJ_y+J_yJ_x)xy]\\&=\frac{1}{2}kr^2+\alpha(3J_z^2-2)+\frac{1}{2}\beta(J_+^2+J_-^2)(x^2-y^2)\\&\quad-i\beta(J_+^2-J_-^2)xy.\end{aligned} \tag{19}$$

For illustrative purposes we will assume that α and $\beta\sigma^2$ are small compared to the phonon energy $\hbar\omega$. Here $\sigma^2=\langle x^2\rangle=\langle y^2\rangle$, where the averages are taken in the ground state. In that case, in addition to the quantum number P, the total number of phonons N is a good quantum number. However, we emphasize that in our numerical work,[18] we do not make this approximation. Equation (10) assumes that J is a good quantum number but mixes states with different numbers of phonon excitations. We should mention that the toy model assumes that the molecule has minimal potential energy

TABLE I. Two-dimensional harmonic oscillator wave functions.

$E/(\hbar\omega)$	$(dE/d\gamma)_{\gamma=0}$	m[a]	ψ	$\psi(x,y)$[b]
1	$8\sigma^4$	0	(0,0)	1
2	$24\sigma^4$	1	$(1,i)$	$x+iy$
2	$24\sigma^4$	−1	$(1,-i)$	$x-iy$
3	$56\sigma^4$	0	$[(2,0)+(0,2)]$	$(r^2/\sigma^2)-2$
3	$48\sigma^4$	2	$[(2,0)-(0,2)+i\sqrt{2}(1,1)]$	$(x+iy)^2/\sigma^2$
3	$48\sigma^4$	−2	$[(2,0)-(0,2)-i\sqrt{2}(1,1)]$	$(x-iy)^2/\sigma^2$
4	$96\sigma^4$	1	$[\sqrt{3}(3,0)+(1,2)]$	$[(x+iy)/\sigma][(r^2\sigma^2)-4]$
4	$96\sigma^4$	−1	$[\sqrt{3}(0,3)+(2,1)]$	$[(x-iy)/\sigma][(r^2/\sigma^2)-4]$
4	$80\sigma^4$	3	$[(3,0)-\sqrt{3}(1,2)]+i\sqrt{3}(2,1)-i(0,3)$	$[(x+iy)/\sigma]^3$
4	$80\sigma^4$	−3	$[(0,3)-\sqrt{3}(2,1)]-i\sqrt{3}(2,1)+i(0,3)$	$[(x-iy)/\sigma]^3$

[a]In cylindrical coordinates the ϕ-dependence is through the factor $e^{im\phi}$.

[b]The wave function contains, in addition to the factors listed, $\exp[-(x^2+y^2)/(4\sigma^2)]$ as well as a normalization factor.

when it on the axis of the tube. For small [e.g., (9,0) tubes] this assumption is justified. For larger tubes, the minimal potential energy occurs for a nonzero value of r and the molecule is dominantly off center. We will later treat that case using a different model.

C. Results of the toy model

We now discuss the results of the toy model assuming that the number of phonons is a good quantum number. We note that all the energy expressions given below are with respect to $BJ(J+1)$ with $J=1$.

1. Zero phonon manifold

We first consider the manifold of the states having $J=1$ with zero phonons. One finds that the energy is diagonal in J_z with

$$E(J_z)=\alpha(3J_z^2-2), \tag{20}$$

so that (if α is positive) one has the singlet $J_z=0$ state lower than the doublet $J_z=\pm 1$ states by an energy separation of 3α. One may visualize this as the energy difference between a state for which the molecule is in the phonon ground state and is oriented parallel to the axis and the two states when the molecule is in the phonon ground state and is oriented transversely to the axis. For later use we tabulate these wave functions in Table II.

2. One-phonon manifold without rotation-translation coupling

If we set $\beta=0$ in the toy model of Eq. (19), then essentially we have independent oscillation of molecules which have fixed orientation. Then if n_x and n_y are the vibrational quantum numbers, we see that in the one-phonon manifold $(n_x+n_y=1)$ we have

$$E(n_x,n_y,J_z)=2\hbar\omega+\alpha(3J_z^2-2), \tag{21}$$

so that the lowest energy state (if $\alpha>0$) is doubly degenerate and the excited state is fourfold degenerate, as is shown in Fig. 4.

3. One-phonon manifold with rotation-translation coupling

The unphysical aspect of the energy level scheme we just found for the one-phonon manifold is that it does not take into account that the molecular orientation ought to be correlated with the translational motion. If the molecule translates near the wall, then the molecule should preferentially be parallel to the wall. This means that the orientation of the molecule has to be correlated with the translational motion. This effect will be greater the more strongly the wall potential affects the motion of the molecule.

In terms of number operators n_x and n_y which are the number of phonon excitations in the x and y directions, respectively, and $a_x^\dagger$ and $a_y^\dagger$ which are creation operators for

TABLE II. Wave functions for rotation-vibration for $J=1, n_x=n_y=0$.

Energy[a]	P[b]	Wave function $n_x=0, n_y=0$		
		$J_z=+1$	$J_z=0$	$J_z=-1$
-2α	0	0	1	0
α	1	1	0	0
α	−1	0	0	1

[a]We tabulate the energy relative to $\hbar\omega$.

[b]P defines the transformation of the wave function under a global rotation, as explained in connection with Eq. (11).

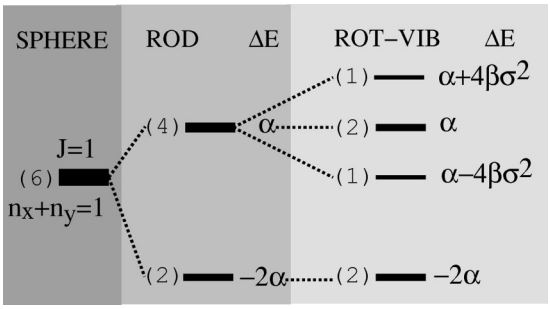

FIG. 4. Removal of the degeneracy in the energy level scheme of the one-phonon ($J=1$) manifold according to the Hamiltonian of Eq. (22). The diagram labeled "sphere" is for a spherical molecule for which $\alpha=\beta=0$. That labeled "rod" is for decoupled rotations and translations of a rodlike molecule for which $\alpha\neq 0$, but $\beta=0$. That labeled "rot-vib" is for translation-rotation coupling with $\beta\neq 0$.

these excitations, we may write the Hamiltonian for the one-phonon ($J=1$) manifold as

$$\mathcal{H}=\hbar\omega(n_x+n_y+1)+\alpha(3J_z^2-2)+\sigma^2\beta[(J_+^2+J_-^2)(n_x-n_y) - i(J_+^2-J_-^2)(a_x^\dagger a_y+a_y^\dagger a_x)]. \quad (22)$$

This gives the energy level scheme shown in the rightmost panel of Fig. 4. The wave functions are given in Table III and we discuss them now. First of all, in a classical picture, we would argue that the molecule can oscillate equivalently in each of the two coordinate directions transverse to the cylinder. In each of these two cases the molecule can assume three inequivalent orientations because the directions (a) along the axis of the tube, (b) parallel to the directions of spatial oscillation, and (c) transverse to the direction of spatial oscillation are all inequivalent to one another. This argument predicts that the six states form three doubly degenerate energy levels. Quantum mechanically the situation is different. In Fig. 4 we show the energy levels when no dynamical mixing between rotations and translations is allowed, i.e., for $\beta=0$. In this limit the six states form a degenerate doublet and a degenerate quartet. When translation-rotation mixing is allowed, i.e., for $\beta\neq 0$, we now have the generic case of two doublets and two singlets, as shown in Fig. 4. The wave functions are shown in Fig. 5. (It is interesting to note that it is not obvious that the wave functions for $P=+2$ and $P=-2$ are related by symmetry.)

4. Two-Phonon manifold with rotation-translation coupling

Actually, because the dependence on r of the matrix elements in Eq. (19) was taken to be either constant or proportional to r^2, the representation of Eq. (22) is valid within any manifold of fixed total number of phonons and ($J=1$). The removal of the degeneracy in the energy level scheme of the two-phonon (i.e., $n_x+n_y=2$) and ($J=1$) manifold according to the Hamiltonian of Eq. (22) is shown in Fig. 6. The eigenfunctions and eigenvalues for this manifold including anharmonicity are listed in Table IV.

The results obtained by numerically solving the eigenvalue problem of Eq. (10) using the WS77 potential are given in the last column of Table V.[18] To understand the meaning of this spectrum, we relate these results to those of the toy model when the parameters of the toy model are suitably chosen. For a good fit we allow the constants α and β to depend on the total number of phonons N. (This dependence reflects the fact that the dependence of the parameters of the toy model on r is arbitrary and unrealistic.) In this simple model we also include the anharmonic term γr^4 which we treat within first order perturbation theory. We determine the best parameters for the toy model by making a least squares fit of the numerically determined energy levels to those of the toy model and these parameters as well as the results of this fit are given in Table. V. The fact that α_N depends on N indicates that we should probably replace α by αr^2. Also the fact that the splitting of the two phonon mani-

TABLE III. Wave functions for rotation-vibration for $J=1$, $n_x+n_y=1$.

Energy[a]	P[b]	Wave function					
		$n_x=1,n_y=0$			$n_x=0,n_y=1$		
		$J_z=+1$	$J_z=0$	$J_z=-1$	$J_z=+1$	$J_z=0$	$J_z=-1$
$\alpha+4\sigma^2\beta$	0	$\frac{1}{2}$	0	$\frac{1}{2}$	$-\frac{1}{2}i$	0	$\frac{1}{2}i$
$\alpha-4\sigma^2\beta$	0	$\frac{1}{2}$	0	$-\frac{1}{2}$	$-\frac{1}{2}i$	0	$-\frac{1}{2}i$
-2α	1	0	$\frac{1}{\sqrt{2}}$	0	0	$\frac{1}{\sqrt{2}}i$	0
-2α	-1	0	$\frac{1}{\sqrt{2}}$	0	0	$-\frac{1}{\sqrt{2}}i$	0
α	2	$\frac{1}{\sqrt{2}}$	0	0	$\frac{1}{\sqrt{2}}i$	0	0
α	-2	0	0	$\frac{1}{\sqrt{2}}$	0	0	$-\frac{1}{\sqrt{2}}i$

[a]We tabulate the energy relative to $2\hbar\omega$.

[b]P defines the transformation of the wave function under a global rotation, as explained in connection with Eq. (11).

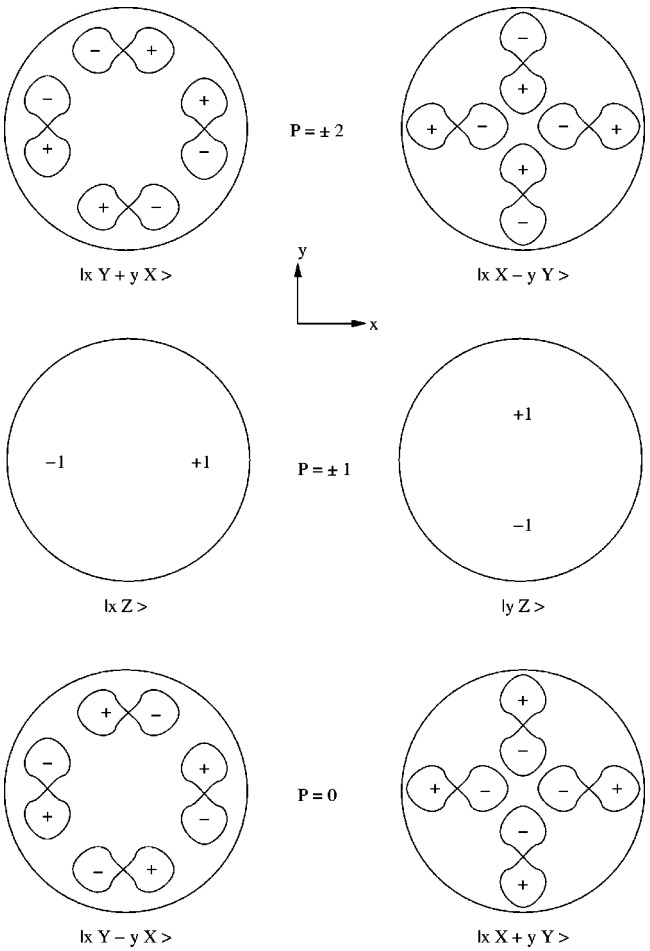

FIG. 5. Translation-rotation wave functions for a $(J=1)$ with one phonon when there is dynamical mixing of translations and rotations. Here the plane of the paper is the x-y plane and each figure eight represents an $|X\rangle$ or $|Y\rangle$ orientational wave function and the sign associated with each lobe of this p-like function is indicated. For the $|Z\rangle$ orientational function (which would have the figure eight coming out of the page) we indicate the sign of the lobe in front of the page. Each orientational wave function is multiplied by a translational wave function $|x\rangle$ or $|y\rangle$, where, for instance, $|x\rangle \sim x \exp[-\frac{1}{4}(x/\sigma)^2]$. The presence of a phonon in the r_α coordinate thus causes the wave function to be an odd function of r_α, as one sees in the diagrams. One sees that the $P=0$ wave functions are invariant under rotation by $\pi/2$. (In fact, they are angular invariants.) From the states labeled with nonzero values of P, one can form the complex linear combinations which transform as $e^{iP\phi}$ when the position and orientation of the molecule are simultaneously rotated about the symmetry axis. Although it is far from obvious, the two states labeled $P=2$ are degenerate in energy. The two $P=0$ states have different energy, in general. So quantum mechanics predicts the six state manifold to consist of two doublets (one for $P=\pm 1$ and one for $P=\pm 2$) and two singlets (for $P=0$).

fold is not perfectly reproduced by the toy model indicates that the anharmonicity energy is not simply proportional to r^4. Nevertheless the close agreement between our numerical results and those of the toy model indicates that this model provides a useful simple picture of translation-rotation coupling.

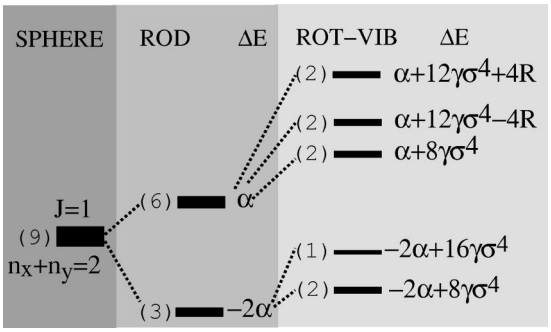

FIG. 6. Removal of the degeneracy in the energy level scheme of the two-phonon $(J=1)$ manifold according to the Hamiltonian of Eq. (22). The diagram labeled ''sphere'' is for a spherical molecule for which $\alpha=\beta=0$. That labeled ''rod'' is for decoupled rotations and translations, but with $\alpha\neq 0$. That labeled ''rot-vib'' is for anharmonic and translation-rotation coupling with $\beta\neq 0$. Here $R=\sqrt{\gamma^2\sigma^8+2\beta^2\sigma^4}$.

5. Summary

We can summarize the systematics of the rotation-translation spectrum of the toy model we have introduced. We first consider the harmonic $\gamma=0$ case and then discuss the effect of introducing anharmonicity. In the N-phonon sector the harmonic phonon wave functions give rise to states proportional to $(x+iy)^N$. Combining these with a $J_z=1$ state gives a unique $P=N+1$ state. This state will be degenerate with the similar $P=-N-1$ state. In the toy model these states have energy $(N+1)\hbar\omega+\alpha$. Adding anharmonicity shifts the energy of these two states, but their degeneracy is generic.

Harmonic phonon states which transform as $(x+iy)^{N-2k}$ will uniquely combine with $J_z=0$ states to form states for which $P=(N-2k)$ and which have energy $(N+1)\hbar\omega-2\alpha$. In analogy with Fig. 4, anharmonicity splits

TABLE IV. Wave functions for $J=1, n_x+n_y=2$ with anharmonic (scaled with γ) and rotation-translation coupling (scaled with β).

P	Wave function[a]	Energy[b]
0	$\|m=0;M=0\rangle$	$-2\alpha+16\gamma\sigma^4$
1	$[\|m=2;M=-1\rangle+\|m=0;M=1\rangle]/\sqrt{2}$	$\alpha+12\gamma\sigma^4+4R$
−1	$[\|m=-2;M=1\rangle+\|m=0;M=-1\rangle]/\sqrt{2}$	$\alpha+12\gamma\sigma^4+4R$
1	$[\|m=2;M=-1\rangle-\|m=0;M=1\rangle]/\sqrt{2}$	$\alpha+12\gamma\sigma^4-4R$
−1	$[\|m=-2;M=1\rangle-\|m=0;M=-1\rangle]/\sqrt{2}$	$\alpha+12\gamma\sigma^4-4R$
2	$\|m=2;M=0\rangle$	$-2\alpha+8\gamma\sigma^4$
−2	$\|m=-2;M=0\rangle$	$-2\alpha+8\gamma\sigma^4$
3	$\|m=2;M=1\rangle$	$\alpha+8\gamma\sigma^4$
−3	$\|m=-2;M=-1\rangle$	$\alpha+8\gamma\sigma^4$

[a]Here M indicates a wave function for which $J_z=M$. The states indicated by m are the phonon states in the cylindrical gauge and are listed in Table I.

[b]Here $R=\sqrt{\gamma^2\sigma^8+2\beta^2\sigma^4}$. Also these are energies relative to $2B+3\hbar\omega+40\gamma\sigma^4$.

TABLE V. Energy levels in meV for the toy model for a ($J=1$) hydrogen molecule inside of a (9,0) tube, compared to numerical calculations based on Eq. (10): The parameters (in meV) are $\alpha_0=2.82$. $\alpha_1=3.56$, $\alpha_2=4.32$, $\beta_1\sigma^2=0.59$, $\beta_2\sigma^2=0.55$, $\gamma\sigma^4=0.29$, and $\hbar\omega=27.36$.

P	Toy Model Energy[a,b]	Energy[a] (Numeric)
0	0	0
±1	$3\alpha_0=8.46$	8.46
0	$2\alpha_0+\alpha_1+4\beta_1\sigma^2+\hbar\omega=38.92$	39.01
0	$2\alpha_0+\alpha_1-4\beta_1\sigma^2+\hbar\omega=34.20$	34.29
±1	$2\alpha_0-2\alpha_1+\hbar\omega=25.88$	25.89
±2	$2\alpha_0+\alpha_1+\hbar\omega=36.56$	36.56
0	$2\alpha_0-2\alpha_2+4\delta+2\hbar\omega=56.36$	55.67
±1	$2\alpha_0+\alpha_2+3\delta+4R+2\hbar\omega=71.68$	71.13
±1	$2\alpha_0+\alpha_2+3\delta-4R+2\hbar\omega=64.64$	64.12
±2	$2\alpha_0-2\alpha_2+8\gamma\sigma^4+2\hbar\omega=54.04$	53.53
±3	$2\alpha_0+\alpha_2+8\gamma\sigma^4+2\hbar\omega=67.00$	66.35

[a]The zero of energy is taken to be the lowest $P=0$ level.
[b]Here $R=\sqrt{\gamma^2\sigma^8+2\beta_2^2\sigma^4}$.

these states into doublets of $+P$ and $-P$ and, if P is even, a singlet for $P=0$.

The rotation-translation coupling (proportional to β) influences the states with $P=N-1$, $P=N-3$, etc. For positive P one has two eigenstates made from linear combinations of states of the form $\phi_1\equiv(x+iy)^{P+1}|J_z=-1\rangle$ and $\phi_2\equiv(x+iy)^{P-1}|J_z=+1\rangle$. Since the rotation translation coupling interaction proportional to $xy(J_+^2-J_-^2)$ has matrix elements between these two states, the eigenstates $\phi_1\pm\phi_2$ will be split by an amount proportional to $\beta\sigma^2$ and this splitting will be modified by anharmonicity. Obviously, this scenario indicates that one can not understand the degeneracies of the states of a hydrogen molecule in confined geometry without considering the effect of rotation-translation coupling.

V. MEXICAN HAT POTENTIAL

Here we discuss the case when the minimum of the potential $V_0(r)$ occurs for nonzero r as happens for H_2 molecules inside 10×10 tubes or for H_2 molecule in a bound state outside any tube. We start from Eq. (10). To see what this equation yields, we first consider its solutions for a ($J=0$) molecule. We have solved the eigenvalue problem of Eq. (10) numerically on a mesh of points for a 10×10 tube.[18] The results shown in Fig. 7(a) indicate two different regimes for the dependence of the energy levels on the quantum number P. For the low-lying energy states it is quadratic and then gradually becomes linear as the energy of the states increase.

It is possible to understand the quadratic behavior of energy levels versus the quantum number P based on a simple idealized model. Assuming $V_0(r)$ can be replaced by a harmonic oscillator potential, Eq. (10) becomes essentially

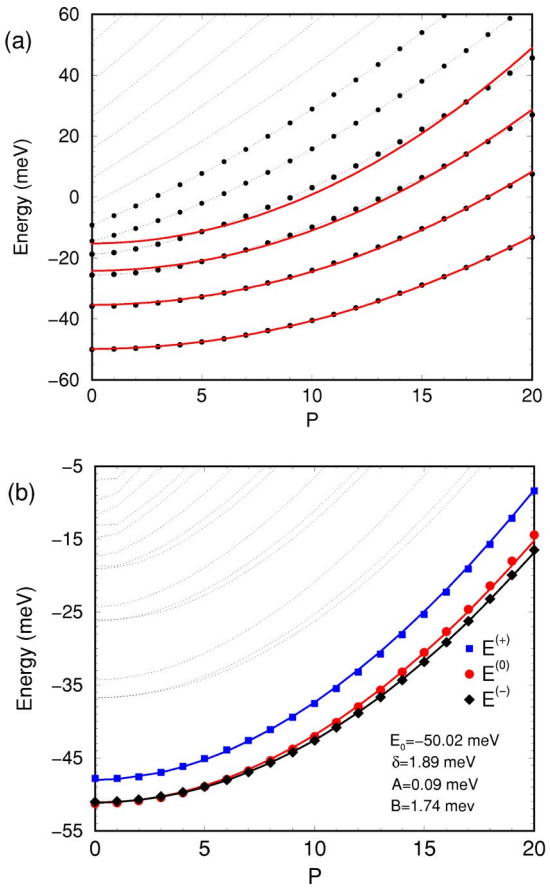

FIG. 7. The energy levels of of an H_2 molecule with ($J=0$) (a) and ($J=1$) (b) inside a (10,10) nanotube versus quantum number P. The symbols and the dotted lines are obtained from numerics and the solid lines are fit based on the simple models as discussed in the text, indicating that a few of the lowest energy levels can be understood from these simple models. For the case of ($J=1$) hydrogen (bottom), for each P we have now three energies, which are split by about 3 meV (comparable to 2.6 meV observed for H_2 on graphite). We note that for both ($J=0$) and ($J=1$) cases, only $N=0,1$, and 2 phonon levels can be safely identified. The inset to the lower panel gives the fitted values of the parameters of Eq. (28). In the lower panel, the energy is with respect to $BJ(J+1)$.

$$\left[-\frac{\hbar^2}{2m}\frac{\partial^2}{\partial r^2}+\frac{\hbar^2P^2}{2mr^2}+E_0+\frac{1}{2}k(r-r_0)^2\right]f_P^{(\alpha)}(r)=E_P^{(\alpha)}f_P^{(\alpha)}(r). \tag{23}$$

In writing this result we dropped the term linear in the derivative. This term does not contribute to the energy in first-order perturbation theory. When we treat the term in P^2 perturbatively, this equation leads to a harmonic oscillator spectrum with

$$E_P^{(N)}=E_0+\left(N+\frac{1}{2}\right)\hbar\omega+\frac{\hbar^2P^2}{2m}\left\langle\frac{1}{r^2}\right\rangle, \tag{24}$$

where $\omega=\sqrt{k/m}$ and $\langle X\rangle$ here indicates an average of X over the radial wave function.

The gray solid lines in Fig. 7a shows the results based on this model and the points are from the numerical exact results, indicating that our idealized model successfully describes the low-lying energy spectrum. Here $\hbar\omega$ is of order 14 meV and and the quantum of tangential kinetic energy $\langle\hbar^2/(2mr^2)\rangle$ is about 0.1 meV. Curiously, this spectrum is reminiscent of the vibration-rotation spectrum of a diatomic molecule.[19] Finally as we go away from the ground state, the simple model is not enough to explain the observed behavior. We note that the spacing between the energy levels is not constant (probably due to an anharmonic contribution to the potential) and the dependence on the P becomes almost linear.

We next discuss the solution of Eq. (10) for a ($J=1$) H_2 molecule. Figure 7(b) shows the results obtained numerically.[18] We will interprate numerical results using a simple model which includes the translation-rotation coupling (as embodied by the v_L^M's). We expect the radial wave functions to be Gaussians centered about $r=r_0$. Indeed in the terms containing $v_L^M(r)$, we will make the replacement

$$v_L^M(r)\rightarrow\langle v_L^M(r)\rangle. \tag{25}$$

[To a good approximation these averages can be calculated from the ($J=0$) wave function.] In what follows we set

$$\langle v_2^M(r)\rangle = w_M \tag{26}$$

for $M=0$ and $M=2$. Then, if we set $r=r_0+x$, Eq. (10) may be approximated as

$$\left[-\frac{\hbar^2}{2m}\frac{\partial^2}{\partial x^2}+\frac{\hbar^2(P+M)^2}{2mr_0^2}+E_0+\frac{1}{2}k(x-r_0)^2\right]f_{M,P}^{(\alpha)}(x) - \frac{1}{\sqrt{2\pi}}\sum_{M'} C(121;M-M',M')w_{M'}f_{M-M',P}^{(\alpha)}(x) = E_P^{\alpha}f_{M,P}^{(\alpha)}(x), \tag{27}$$

where the Clebsch-Gordan coefficients assume the values $C(121;L,0)=(3L^2-2)/\sqrt{10}$ and $C(121;-1,2)=\sqrt{3/5}$. For each value of N (the number of radial phonons) and P (the number of tangential excitations) the Hamiltonian is the following three-dimensional matrix (where the rows correspond to $J_z=-1$, $J_z=0$, and $J_z=+1$, in that order):

$$\mathcal{H}(N,P)=[E_0+N\hbar\omega]\mathcal{I}+\begin{bmatrix} \frac{1}{3}\delta+A(P-1)^2 & 0 & B \\ 0 & -\frac{2}{3}\delta+AP^2 & 0 \\ B & 0 & \frac{1}{3}\delta+A(P+1)^2 \end{bmatrix}, \tag{28}$$

where $\mathcal{I}$ is the unit matrix, $A=\langle\hbar^2/(2mr_0^2)\rangle$, $\delta=-3w_0/\sqrt{20\pi}$, and $B=-w_2\sqrt{3/10\pi}$. For fixed values of N and P we have the three energy eigenvalues

$$E^{(0)}=E_0+N\hbar\omega-\frac{2}{3}\delta+AP^2,$$

$$E^{(\pm)}=E_0+N\hbar\omega+\frac{1}{3}\delta+A(P^2+1)\pm\sqrt{4A^2P^2+B^2}. \tag{29}$$

In Fig. 7(b) we show the spectrum of a ($J=1$) molecule obtained numerically from Eq. (10) as a function of P. Our numerical results indicate the phonon number N is a good quantum number and can so be identified only for $N<3$. Accordingly, we limit our detailed interpretation in terms of the model of Eq. (28) to $N=0$. For each value of P there are three energy eigenvalues, two of which are close in energy. These corresponds to the case where the H_2 molecule is oriented parallel to the tube surface (i.e., t and p orientations in Fig. 3). The third energy corresponds to the orientation perpendicular to the tube surface (i.e., r radial orientation shown in Fig. 3). This orientation has an energy about 3 meV near than that of the other two orientations, and is comparable to 2.6 meV observed for H_2 on graphite.[12] Figure 7(b) shows also the result of the simple model of Eq. (28). The values of A, B, and δ used to get a good fit are given in the figure. The value of A (0.092 meV) is not very different from the value $\hbar^2/(2mr_0^2)=0.087$ one gets from the value of $r=r_0=3.46$ Å at the minimum of the potential. Thus the numerical results are easily understood in terms of our simple toy model.

VI. EXPERIMENTAL OBSERVATION OF THE ENERGY SPECTRUM

Here we make some remarks concerning the observation of these modes via inelastic neutron scattering. Specifically we consider the energy loss spectrum in the neutron time-of-flight spectrum. (This technique has been used to probe local excitation of H_2 molecules in the octahedral sites of C_{60}.[11]) We start be recalling the results for the cross section for inelastic neutron scattering of H_2 molecules. When the very small coherent (i.e., nuclear spin independent) scattering is neglected, the result is

$$\frac{\partial^2\sigma}{\partial\Omega\,\partial E}=\frac{k'}{k}[Nx\mathcal{S}_{1\rightarrow1}+Nx\mathcal{S}_{1\rightarrow0}+N(1-x)\mathcal{S}_{0\rightarrow1}], \tag{30}$$

where $\mathbf{k}$ ($\mathbf{k}'$) is the wave vector of the incident (scattered) neutron, N is the total number of H_2 molecules in the target, x is the fraction of H_2 molecules which have odd J (i.e., are ortho molecules), and the subscripts indicate the partial cross sections due to ortho molecules, to ortho-para conversion, and to para-ortho conversion, respectively. When the sum over nuclear spin states is performed, these partial cross sections are given by

$$\mathcal{S}_{0\to 1,j}=\frac{3}{4}(b')^2\sum_{J_i=0,J_f=1} P_i\delta(E-E_i+E_f)\times\left|\langle f|e^{i\kappa\cdot\mathbf{R}_j}\sin\left(\frac{1}{2}\kappa\cdot\rho\right)|i\rangle\right|^2$$

$$\mathcal{S}_{1\to 0,j}=\frac{1}{4}(b')^2\sum_{J_i=1,J_f=0} P_i\delta(E-E_i+E_f)\times\left|\langle f|e^{i\kappa\cdot\mathbf{R}_j}\sin\left(\frac{1}{2}\kappa\cdot\rho\right)|i\rangle\right|^2$$

$$\mathcal{S}_{1\to 1,j}=\frac{1}{2}(b')^2\sum_{J_i=1,J_f=1} P_i\delta(E-E_i+E_f)\times\left|\langle f|e^{i\kappa\cdot\mathbf{R}_j}\cos\left(\frac{1}{2}\kappa\cdot\rho\right)|i\rangle\right|^2, \tag{31}$$

where $\kappa=\mathbf{k}'-\mathbf{k}$, R_j is the center of mass of the jth H_2 molecule, and ρ is the vector displacement of one proton relative to the other proton in the H_2 molecule. Here b' is the incoherent cross section of the proton and P_i is the canonical probability of state i. To deal with molecular orientations for molecules where J is at most unity, we write

$$\cos\left(\frac{1}{2}\kappa\cdot\hat{\rho}\right)=j_0\left(\frac{1}{2}\kappa\rho\right)-4\pi j_2\left(\frac{1}{2}\kappa\rho\right)\sum_\mu Y_2^\mu(\hat{\kappa})Y_2^\mu(\hat{\rho})^*$$

$$\sin\left(\frac{1}{2}\kappa\cdot\hat{\rho}\right)=4\pi j_1\left(\frac{1}{2}\kappa\rho\right)\sum_\mu Y_1^\mu(\hat{\kappa})^*Y_1^\mu(\hat{\rho}), \tag{32}$$

where j_n is a spherical Bessel function. We will assume that κ is small enough that the term in j_2 can be neglected. Since it is not trivial to obtain a meaningful result which properly contains the Debye-Waller factor, we proceed simply, as follows. From the numerical solution on a mesh of points we obtain the family of wave functions (each one denoted $|J,P;\alpha\rangle$), for which J and P are good quantum numbers and $\alpha=1,2,3,\ldots$. (In limiting cases one may replace the single index α by two indices N and γ, where N, the number of phonons, is nearly a good quantum number.) If we label the radial mesh points by $k=1,2,3,\ldots$, then we have

$$|J,P;\alpha\rangle=\frac{\Sigma_{\mu=-J}^{J}\Sigma_k c_{J,P}^{(\alpha)}(k,\mu)e^{-i(P+\mu)\phi_r}\sqrt{r_k}|r_k\rangle|J,J_z=\mu\rangle}{[2\pi\Sigma_{\mu=-J}^{J}\Sigma_k|c_{J,P}^{(\alpha)}(k,\mu)|^2 r_k]^{1/2}}. \tag{33}$$

Here $|r_k\rangle$ (and later $\langle r_k|$) is a wave function of unit amplitude at the position r_k. Also the $c_{J,P}^{(\alpha)}(k,\mu)$'s are the set of coefficients (for fixed J, P, and α) which are obtained by the numerical solution of the $(2J+1)$-component radial eigenvalue problem on a set of mesh points $\{r_k\}$. This discretized eigenvalue problem involves diagonalization of nonsymmetric matrix. (The radial equation gives rise to a Hermitian problem only if proper account is taken of the radial weight function.) The numerical program takes no account of any weight factor, but rather normalizes these wave functions by requiring that the sum of the squares of their coefficients be unity. Since we always wish to define inner products with a weight factor r_k, we will explicitly include a factor r_k when we take inner products. Then if X is a quantity which is local in r and ϕ_r but may be off diagonal in J and/or J_z, we express its matrix element between such numerically obtained wave functions as

$$\langle J',P';\beta|X|J,P;\alpha\rangle\equiv\frac{\int_0^{2\pi}d\phi_r\Sigma_{k,\mu,\mu'}\langle J',J_z=\mu'|X(r_k,\phi_r)|J,J_z=\mu\rangle r_k c_{J',P'}^{(\beta)}(k,\mu')^* c_{J,P}^{(\alpha)}(k,\mu)e^{i(P'-P+\mu'-\mu)\phi_r}}{2\pi[\Sigma_{k,\mu}|c_{J,P}^{(\alpha)}(k,\mu)|^2 r_k\Sigma_{k',\mu'}|c_{J',P'}^{(\beta)}(k',\mu')|^2 r_{k'}]^{1/2}}. \tag{34}$$

Here μ' assumes integer values between $-J'$ and $+J'$ and μ integer values between $-J$ and $+J$.

To evaluate the cross sections, the major problem is to evaluate the matrix element, which we may call $\langle f|X|i\rangle$. We will not discuss all possible transitions (which are shown in Fig. 4 of I). Instead we will focus on the neutron energy loss spectrum due to (a) para to ortho conversion or (b) radial phonon creation on an ortho molecule.

A. Para to ortho conversion

For neutron energy loss due to para to ortho conversion, we need the matrix element of

$$X=4\pi j_1\left(\frac{1}{2}\kappa\rho\right)\exp(i\kappa\cdot\mathbf{R}_j)\sum_\nu Y_1^\nu(\kappa)Y_1^\nu(\hat{\rho})^* \tag{35}$$

and for simplicity we consider the case when κ is perpen-

dicular to the cylindrical axis of the nanotube. Then we may as well place κ along the local x axis. Also the center of mass of molecule j is at $\mathbf{r}_k$ relative to the axis of the tube at position $\mathbf{R}_j^{(0)}$ which contains the jth molecule. Then we may write

$$X=\sqrt{6\pi}j_1\left(\frac{1}{2}\kappa\rho\right)e^{i\kappa\cdot\mathbf{R}_j^{(0)}}e^{i\kappa r_k\cos\phi_r}[Y_1^{-1}(\hat{\rho})-Y_1^1(\hat{\rho})]. \quad (36)$$

At low temperature the initial state (whose energy is denoted E_i) will be the ground state for $J=0$ and for a small value of P (which we denote P_i). Thus

$$S_{0\to1}=\frac{9}{2}\pi\left[b'j_1\left(\frac{1}{2}\kappa\rho\right)\right]^2 Z^{-1}\times\sum_{i,f}e^{-E_i/(kT)}\delta[E-E_i+E_f]M_{if}, \quad (37)$$

where E_f is the energy of the $(J=1)$ final state, and $Z=\Sigma_i\exp[-E_i/(kT)]$, and

$$M_{if}=\left|\frac{\int_0^{2\pi}d\phi_r\Sigma_{k,\mu}\langle J=1,J_z=\mu|Y_1^1(\hat{\rho})-Y_1^{-1}(\hat{\rho})|J=0,J_z=0\rangle e^{i\kappa r_k\cos\phi_r}e^{i(P_f-P_i+\mu)\phi_r}r_k c_f(k,\mu)^* c_i(k)}{2\pi[\Sigma_k|c_i(k)|^2 r_k\Sigma_{k,\mu}|c_f(k,\mu)|^2 r_k]^{1/2}}\right|^2$$

$$=\frac{\left|\Sigma_k[J_{P_f-P_i+1}(\kappa r_k)c_f(k,1)^*-J_{P_f-P_i-1}(\kappa r_k)c_f(k,-1)^*]r_k c_i(k)\right|^2}{4\pi\Sigma_k|c_i(k)|^2 r_k\Sigma_{k,\mu}|c_f(k,\mu)|^2 r_k}, \quad (38)$$

where $J_n(x)$ is a Bessel function and $c_i(k)$ is the value of $c_{J,P}^{(\alpha)}(k)$ for the initial state and $c_f(k)$ is the value of $c_{J',P'}^{(\beta)}(k',\mu')$ for the final state.

We now discuss the qualitative meaning of this result. We calculated $S_{0\to1}$ for several temperatures and the results are plotted in Fig. 8(a). At zero temperature the initial state has $P_i=0$. So the energy loss is zero up to the cut-off energy which is the energy of para-to-ortho conversion. For small temperatures, the cross section does not appear discontinuously, but turns on rapidly over a range of energy of order kT. The first para-to-ortho (i.e., $J=0$ to $J=1$) transition is observed at energies about 16.8 and 13.6 meV with approximately one-to-two intensity ratio (corresponding to a splitting of 3.2 meV between $J=1,M=0$ and $J=1,M=\pm1$ states, respectively). The center of gravity of the $J=1$ levels gives the average para-ortho conversion energy $E_c=14.67$ meV. This result represents only a small amount of downward shift of 0.03 meV from the free molecule value of 14.7 meV.

We note that there are several neutron scattering experiments reporting the para-to-ortho transition.[9,10] The observed splitting is about 1 meV, suggesting the idea that in those experiments hydrogen molecules were probably not inside the nanotubes. The calculated para-to-ortho splitting of 3.2 meV is slightly larger than the 2.6 meV splitting observed for H_2 on graphite.[12]

In addition to the sharp para-to-ortho rotational transitions, Fig. 8(a) also indicates several broad radial phonon transitions at energies about 15 and 30 meV (similar values to those of H_2 trapped in solid C_{60}). Finally we note that there are many lines in the spectrum due to transition between different tangential phonon states (i.e., P quantum number). However, their observation could be problematic due to experimental energy resolution (which would be worse at high energies than FWHM of 0.5 meV used in Fig. 8).

B. Ortho Cross Section

Here we discuss the scattering from an ortho H_2 molecule. As before, the major problem is the calculation of the matrix element. In analogy with the previous results we write

$$S_{1\to1}=\frac{1}{2}\left[b'j_0\left(\frac{1}{2}\kappa\rho\right)\right]^2 Z^{-1}\times\sum_{if}e^{-E_i/(kT)}\delta[E-E_i+E_f]M_{if}, \quad (39)$$

where we neglect terms involving $j_2(\frac{1}{2}\kappa\rho)$ and

$$M_{if}=|\langle f|e^{i\kappa r_k\cos\phi_r}|i\rangle|^2. \quad (40)$$

Now for M_{if} we have in the notation of Eq. (38)

$$M_{if}=\left|\frac{\int_0^{2\pi} d\phi_r \sum_{k,\mu} e^{i\kappa r_k \cos\phi_r} e^{i(P_f-P_i)\phi_r} r_k c_f(k,\mu)^* c_i(k,\mu)}{2\pi\left[\sum_{k,\mu}|c_i(k,\mu)|^2 r_k \sum_{k,\mu}|c_f(k,\mu)|^2 r_k\right]^{1/2}}\right|^2 = \frac{\left|\sum_{k,\mu} J_{P_f-P_i}(\kappa r_k) r_k c_f(k,\mu)^* c_i(k,\mu)\right|^2}{\sum_{k,\mu}|c_i(k,\mu)|^2 r_k \sum_{k,\mu}|c_f(k,\mu)|^2 r_k}. \quad (41)$$

Figure 8(b) shows the calculated spectrum ortho cross section $S_{1\to 1}$, indicating many transitions between a large number of states. It is possible to identify the radial phonon transitions for only one and two phonon states as indicated in the figure. On the other hand, the transitions between tangential phonon states (i.e., states with different quantum number P) dominate the calculated spectrum, giving rise to many sharp peaks. Due to experimental energy resolution, it is probably not possible to observe the transition at high energies (say above 20 meV). However, the resolution at energies below around 10 meV could be about 0.5 meV (which is used in Fig. 8) and therefore it may be possible to observe these transitions.

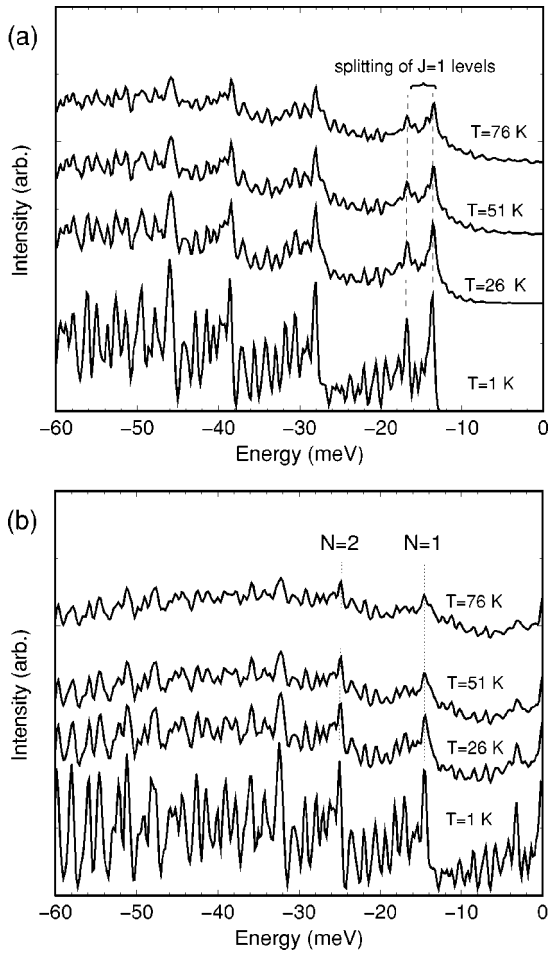

FIG. 8. The calculated neutron cross section (with arbitrary scaling) for para to ortho (a) and ortho to ortho (b) transitions at several temperatures. The neutron wave vector transfer $\boldsymbol{\kappa}$ is taken to be perpendicular to the tube axis with magnitude of 3 Å^{-1}. The peaks are broadened by Gaussians with FWHM of 0.5 meV.

Finally we note that the tangential phonon transitions below 10 meV show a maximum near 3.6 to 4 meV. We can understand this by considering the condition that the neutron wave form become resonant with the wave function of H_2 molecule going around the circumference of the minimum of the Mexican hat. The phase change when the neutron passes through a diamater of the Maxican hat is $2\kappa r_0$, where r_0 is the radius at which the Maxican hat potential is minimal. The phase change of the H_2 molecule going around half a circumference is πP. If we assume an initial state with $P_i=0$, then the resonance condition is $\pi P_f = 2\kappa r_0$. With $\kappa = 3\ \text{Å}^{-1}$ and $r_0 = 3.5$ Å, we find $P_f \approx 6$. Then $E_f - E_i = \hbar^2 P_f^2 \langle (2mr_0)^{-1}\rangle = 0.09 P^2$ meV $= 3.2$ meV, in reasonable agreement with the numerical evaluation.

VII. CONCLUSION

We list the major conclusion from our study of H_2 molecules bound to nanotubes which we treat as smooth cylinders.

We have derived the analog of a radial equation for the Schrödinger equation for the translational and rotational motion of a molecule in cylindrical geometry. This formulation leads to classifying translation-rotation wave functions according to their properties under a global rotation of the molecule about the cylindrical axis.

Using this radial equation, the translation-rotation wave functions for a hydrogen molecule bound either inside or outside a nanotube can be obtained numerically. We also have developed simple toy models which quite accurately reproduce the numerical results, but have the advantage that they elucidate the nature of the translation-rotation dynamics.

Simple classical symmetry arguments fail to predict the correct degeneracies of translation-rotation wave functions. However, the quantum wave functions are easy to understand qualitatively. For instance, for a $J=1$ molecule (such as ortho-H_2), one class of translation-rotation wave functions has the molecule in a $J_z=0$ state (i.e., aligned along the axis of the nanotube) with no admixture from $J_z=\pm 1$. This simplification is a result of the mirror plane perpendicular to axis of the cylinder.

We also suggest that neutron time-of-flight spectra could provide useful confirmation of our results. To that end we have calculated typical spectra that might be observed. These are shown in Fig. 8.

ACKNOWLEDGMENTS

A.B.H. would like to thank NIST for its hospitality during several visits when this work was done. We acknowledge

partial support from the Israel-US Binational Science Foundation (BSF).

APPENDIX A: INCLUSION OF BOTH ANHARMONICITY AND TRANSLATION-ROTATION COUPLING

Here we study the simultaneous effect of anharmonicity and translation rotation coupling for the two-phonon manifold within the toy model. From Table I we see that we may write the anharmonic Hamiltonian $V_{\rm AH}$, which is independent of J_z, as

$$V_{\rm AH}=V_0\mathcal{I}+\frac{8}{3}\gamma\sigma^4\big[2|2,m=0\rangle\langle 2,m=0| -|2,m=2\rangle\langle 2,m=2|-|2,m=-2\rangle\langle 2,m=-2|\big], \tag{A1}$$

where $V_0=152\gamma\sigma^4/3$ and $|2,m\rangle$ is a two-phonon wave function (with energy $3\hbar\omega$) as given in Table I. The translation rotation interaction may be written as

$$V=\alpha[3J_z^2-2]+V', \tag{A2}$$

where

$$V'=\frac{1}{2}\beta[J_+^2(x-iy)^2+J_-^2(x+iy)^2]. \tag{A3}$$

If we write the ground state wave function as

$$|0\rangle=N_{0,0}e^{-(1/4)(x^2+y^2)/\sigma^2}, \tag{A4}$$

then the two phonon eigenstates are

$$|2,m=0\rangle=\frac{1}{2}(X^2+Y^2-2)N_{00}e^{-(1/4)(X^2+Y^2)} \tag{A5}$$

and

$$|2,m=\pm 2\rangle=\frac{1}{2\sqrt{2}}(X+iY)^2N_{00}e^{-(1/4)(X^2+Y^2)}, \tag{A6}$$

where $X=x/\sigma$ and $Y=y/\sigma$. If $\langle\ \rangle$ indicates a ground state average, then we have the evaluation

$$\begin{aligned}\langle 0|(x-iy)^2|2;m=2\rangle &=\sigma^2\left\langle\left(\frac{1}{2}(X^2+Y^2-2)(X-iY)^2\frac{1}{2\sqrt{2}}(X+iY)^2\right)\right\rangle\\ &=4\sqrt{2}\sigma^2,\end{aligned} \tag{A7}$$

so that

$$V'=2\sqrt{2}\beta\sigma^2\big[|2,m=-2\rangle\langle 2,m=0| +|2,m=0\rangle\langle 2,m=2|\big]J_+^2+\text{H.c.}, \tag{A8}$$

where H.c. indicates the Hermitian conjugate of the preceding term. We find the eigenvalues to be those of Table IV.

APPENDIX B: CARTESIAN REPRESENTATION

Here we rewrite in the Cartesian representation the eigenfunctions which were given in Table III in cylindrical coordinates.

$$\begin{aligned}|J_z=0\rangle&=|Z\rangle,\\ |J_z=1\rangle&=-\frac{1}{\sqrt{2}}|X+iY\rangle,\\ |J_z=-1\rangle&=\frac{1}{\sqrt{2}}|X-iY\rangle.\end{aligned} \tag{B1}$$

From Table III the eigenfunctions with energy $\alpha\pm 4\sigma^2\beta$ are

$$\psi_\pm=\frac{1}{2\sqrt{2}}(-|(X+iY)(x-iy)\rangle\mp|(X-iY)(x+iy)\rangle). \tag{B2}$$

So, apart from a phase factor,

$$\begin{aligned}\psi_+&=\frac{1}{\sqrt{2}}|xX+yY\rangle,\\ \psi_-&=\frac{1}{\sqrt{2}}|xY-yX\rangle.\end{aligned} \tag{B3}$$

From Table III the eigenfunctions with energy α are

$$\psi_\pm=-\frac{1}{2}|(x\pm iy)(X\pm iY)\rangle \tag{B4}$$

so that we may take the eigenfunctions to be

$$\begin{aligned}\psi_1&=\frac{1}{\sqrt{2}}|xX-yY\rangle,\\ \psi_2&=\frac{1}{\sqrt{2}}|xY+yX\rangle.\end{aligned} \tag{B5}$$

[1] S. A. FitzGerald, S. Forth, and M. Rinkoski, Phys. Rev. B **65**, 140302 (2002).
[2] K. A. Williams, B. K. Pradhan, P. C. Eklund, M. K. Kostov, and M. W. Cole, Phys. Rev. Lett. **88**, 165502 (2002).
[3] D. G. Narehood, M. K. Kostov, P. C. Eklund, M. W. Cole, and P. E. Sokol, Phys. Rev. B **65**, 233401 (2002).
[4] M. K. Kostov, H. Cheng, R. M. Herman, and M. W. Cole, J. Chem. Phys. **116**, 1720 (2002).
[5] T. Yildirim and A. B. Harris, Phys. Rev. B **66**, 214301 (2002).
[6] Q. Wang and J. K. Johnson, J. Chem. Phys. **110**, 577 (1999).

[7] Q. Wang, S. R. Challa, D. S. Sholl, and J. K. Johnson, Phys. Rev. Lett. **82**, 956 (1999).
[8] M. M. Calbi and M. W. Cole, Rev. Mod. Phys. **73**, 857 (2001).
[9] Y. Ren and D. L. Price, Appl. Phys. Lett. **79**, 3684 (2001).
[10] C. M. Brown, T. Yildirim, D. A. Neumann, M. J. Heben, T. Gennett, A. C. Dillon, J. L. Alleman, and J. E. Fischer, Chem. Phys. Lett. **329**, 311 (2000).
[11] S. A. FitzGerald, T. Yildirim, L. J. Santodonato, D. A. Neumann, J. R. D. Copley, J. J. Rush, and F. Trouw, Phys. Rev. B **60**, 6439 (1999).
[12] A. D. Novaco and J. P. Wroblewski, Phys. Rev. B **39**, 11 364 (1989).
[13] L. Pauling, Phys. Rev. B **36**, 430 (1930).
[14] A. F. Devonshire, Proc. R. Soc. London, Ser. A **153**, 601 (1936).
[15] H. M. Cundy, Proc. R. Soc. London, Ser. A **164**, 420 (1938).
[16] *The Atom-Atom Potential Method*, edited by A. J. Pertsin and A. I. Kitaigorodsky (Springer-Verlag, Berlin, 1986), p. 89.
[17] T. Yildirim and A. B. Harris (unpublished).
[18] The numerical results reported here were obtained by solving the eigenvalue problem on a discrete mesh of points with $dr = 0.025$ Å. The resulting large sparse matrix eigenvalue problem is solved using the package ARPACK. The package is designed to compute a few eigenvalues and corresponding eigenvectors of a general n by n matrix. More information about the code is available at http://www.caam.rice.edu/software/ARPACK
[19] *Spectra of Diatomic Molecules*, 2nd ed., edited by G. Hertzberg (D. Van Nostrand, New York, 1950), p. 150.